A&A, 693, A63 (2025)
https://doi.org/10.1051/0004-6361/202452309

Astronomy & Astrophysics

Distinguishing super-Nyquist frequencies via their temporal variation in γ Doradus stars from continuous photometry

Xuan Wang[1,2,3], Weikai Zong[1,2,3,⋆], Xiao-Yu Ma[4], Stéphane Charpinet[5], Tao Wu[6,7,8,9,3], and Haotian Wang[10]

[1] Institute for Frontiers in Astronomy and Astrophysics, Beijing Normal University, Beijing 102206, PR China
[2] School of Physics and Astronomy, Beijing Normal University, Beijing 100875, PR China
[3] International Centre of Supernovae, Yunnan Key Laboratory, Kunming 650216, PR China
[4] Space Sciences, Technologies and Astrophysics Research (STAR) Institute, Université de Liège, Allée du 6 Août 19C, 4000 Liège, Belgium
[5] IRAP, CNRS, UPS, CNES, Université de Toulouse, 14 Av. Edouard Belin, 31400 Toulouse, France
[6] Yunnan Observatories, Chinese Academy of Sciences, 396 Yangfangwang, Guandu District, Kunming 650216, PR China
[7] Key Laboratory for the Structure and Evolution of Celestial Objects, Chinese Academy of Sciences, 396 Yangfangwang, Guandu District, Kunming 650216, PR China
[8] Center for Astronomical Mega-Science, Chinese Academy of Sciences, 20A Datun Road, Chaoyang District, Beijing 100012, PR China
[9] University of Chinese Academy of Sciences, Beijing 100049, PR China
[10] Institute of Astronomy, KU Leuven, Celestijnenlaan 200D, 3001 Leuven, Belgium

Received 19 September 2024 / Accepted 15 November 2024

ABSTRACT

Given their tendency to mix in with real pulsations, the reflection of super-Nyquist frequencies (SNFs) pose a threat to asteroseismic properties. Although SNFs have been studied in several pulsating stars, a systematic survey remains to be explored. Here, we propose a method for identifying SNFs from *Kepler* and TESS photometry by characterizing their periodic frequency modulations using a sliding Fourier transform. After analyzing long-cadence photometry in the *Kepler* legacy, we identified 304 SNFs in 56 stars from 45 607 frequencies in ∼600 γ Doradus stars, corresponding to a fraction of approximately 0.67% and 9.2%, respectively. Most SNFs were detected in the frequency range of pressure mode over 120 µHz and the fraction of SNF detection increases as frequency up to ∼7%. We found only two potential SNFs mixed with gravity modes in two γ Doradus stars. These findings indicate that SNFs have a negligible impact on global seismic properties, such as those derived from period spacing in γ Doradus stars. However, we stress that SNFs must be carefully and systematically examined by this method in other pulsating stars, particularly δ Scuti and hot B subdwarf stars, to establish a solid foundation for the precise asteroseismolgy of various types of pulsators.

Key words. methods: statistical – techniques: photometric – stars: oscillations

1. Introduction

Asteroseismology, via characterizing the properties of pulsation spectra, is a unique technique used to probe the internal structure and physics of pulsating variables (Aerts 2021). Nowadays, pulsating stars can be found throughout the entire Hertzsprung–Russell diagram (see, e.g., Kurtz 2022), providing opportunities to apply asteroseismology to the different evolutionary stages of stars. Spaceborne observations from missions such as *Kepler*/K2 (Borucki et al. 2010; Howell et al. 2014) and TESS (Ricker et al. 2015) have ushered asteroseismology into a gold era (see, e.g., Aerts 2021), thanks to their high precision and continuous photometry of over one million stars. The sharp frequency resolution and low noise level have led to many achievements in asteroseismology, including the diagnosis of evolutionary stages between red clump and red giant stars (Bedding et al. 2011), the determination of oxygen/carbon abundance in white dwarf stars (Giammichele et al. 2018), and the study of internal magnetism and rotation in highly evolved stars (Fuller et al. 2015; Li et al. 2022; Mosser et al. 2024). Seismic results, in turn, have demonstrated their great potential in advancing various areas such as star-planet systems, galactic archaeology, and the progenitors of supernovae (Huber et al. 2013; Miglio et al. 2021; Bowman 2020).

Among all pulsating stars, γ Doradus (γ Dor) stars, as common classical pulsating variables, significantly benefit from the four-year *Kepler* photometry. As a result, various interesting seismic characteristics have been revealed, which would otherwise not be achieved from ground-based photometry (see, e.g., Van Reeth et al. 2016; Ouazzani et al. 2020; Li et al. 2020). These objects typically have A/F-type spectra, temperatures of 6000−10 000 K, and masses between 1.4 and 2.5 $M_\odot$ (Uytterhoeven et al. 2011). Also, γ Dor stars undergo high-order nonradial gravity (g-mode) pulsations with periods of 0.3−3 days, mainly driven by convective blocking at the base of the envelope convection zone (Guzik et al. 2000). By analyzing their dense oscillation spectra, the period spacing patterns in γ Dor stars reveal critical information about internal physical properties. The practical technique to analyze the period spacing in γ Dor stars was first tested by Van Reeth et al. (2015) and applied to *Kepler* γ Dor stars, leading to the discovery of Rossby modes (Van Reeth et al. 2016), measurements of near-core rotation rates for a bulk of stars (Li et al. 2020), and the detection of pure inertial modes (Ouazzani et al. 2020), etc.

Since a large proportion of the recent developments in the study of γ Dor stars rely on the fine patterns of pulsation spectra, any deviation from the main trend in period spacing may provide new insights into the internal physics at work (see, e.g.,

⋆ Corresponding author; weikai.zong@bnu.edu.cn

Ouazzani et al. 2020). However, an issue that has not yet been explored in γ Dor stars is related to the super-Nyquist frequency, which is by definition higher than the Nyquist frequency (a value determined by sampling exposure). Many γ Dor stars are found to be hybrid pulsators with pressure (p-mode) pulsations that can exceed the Nyquist frequency of *Kepler* long-cadence photometry. Therefore, those high p-mode frequencies will be reflected to the lower frequency region (Murphy et al. 2013) and may be disguised as g-mode pulsations, impacting the reliability of period spacing analysis.

The super-Nyquist frequency and its reflection (hereafter, SNF) of *Kepler* and TESS photometry has been thoroughly investigated by Murphy et al. (2013) and Murphy (2015), who discussed the fact that a SNF can be identified by its profile, appearing as a multiplet due to irregular time sampling. With the same technique, Hey et al. (2019) found six new rapidly oscillating Ap (roAp) stars, whose pulsation periods are much shorter than the *Kepler* photometry of long cadence. Similarly, Chaplin et al. (2014) suggested that SNFs can be used to detect solar-like oscillations, enlarging the sample of solar-like stars for *Kepler*/K2 photometry. Due to frequency range limitations, very rapid oscillations will become SNFs even using the *Kepler* short-cadence photometry, bringing further difficulties in mode discriminant. Careful attention has been paid to several rapid pulsations in hot B subdwarfs and white dwarfs (see, e.g., Baran et al. 2012; Bell et al. 2017). Moreover, SNFs introduce false-alarm amplitude modulation of the real pulsation mode (see, e.g., Bowman et al. 2016), but they can be easily identified by their modulating patterns, which have the same period as the *Kepler* orbit (Zong & Charpinet 2021).

Although SNFs can be recognized by equal-spacing multiplets (Murphy et al. 2013) or periodic patterns of amplitude modulation (Zong & Charpinet 2021), both techniques are challenging with respect to their application in SNF identification for a large sample of γ Dor stars. The former may be obscured in the dense pulsation spectrum, while the latter requires significant computational time to extract modulating information. In this work, we have initiated a dedicated and systematic survey that aims to identify SNFs in *Kepler* γ Dor stars and to evaluate their impact on period spacing. In this paper, we propose a new method to identify SNFs in ~600 γ Dor stars from *Kepler* photometry. The article is structured as follows. A series of simulating experiments are presented in Sect. 2. In Sect. 3, we describe the data sample and methodology, and the results are presented in Sect. 4. Finally, we conclude the discussion in Sect. 5 by addressing the significance and future prospects.

2. Modulation of super-Nyquist frequency

2.1. Theoretical exploration of Nyquist frequency

As noted by Murphy et al. (2013), the sampling time of *Kepler* photometry displays same exposure on board, but it is destroyed by barycentric corrections accounting for the motion of the spacecraft. The corrected time, $t_{s,n}$, for each exposure in the sequence is defined as follows,

$$t_{s,n} = t_n + \tau \cos(\lambda_{\odot,t_n} - \lambda), \tag{1}$$

$$\tau \equiv \frac{a}{c} \cos\beta, \tag{2}$$

where a refers to the semi-major axis of the elliptical orbit, c is the speed of light, λ and β are the ecliptic longitude and latitude of the targeting star, and $\lambda_{\odot,t_n}$ is the geocentric ecliptic longitude of the Sun. Then, t_n represents the equal onboard sampling times as

$$t_n = t_0 + n\Delta t. \tag{3}$$

Here, n is the sequence number, t_0 is the start time of the first exposure, and Δt is the constant exposure time. When substituting Eqs. (2) and (3) into (1), we obtain a corrected sampling interval as:

$$\Delta t_{s,n} = \Delta t - \tau[\cos(\lambda_{\odot,t_{n+1}} - \lambda) - \cos(\lambda_{\odot,t_n} - \lambda)]. \tag{4}$$

In elliptic equation, $\lambda_{\odot,t_n}$ does not explicitly involve time t. Since an analytical expression for $\lambda_{\odot,t_n}$ in terms of t is not available, we can obtain $\lambda_{\odot,t_n}$ through numerical iterative calculations. Equation (4) shows that the time interval $\Delta t_{s,n}$ modulates as sinusoidal waves, which causes the Nyquist frequency, $f_{\mathrm{ny},n}$, to vary over time. This is based on

$$f_{\mathrm{ny},n} = \frac{1}{2\Delta t_{s,n}} = \frac{1}{2\{\Delta t - \tau[\cos(\lambda_{\odot,t_{n+1}} - \lambda) - \cos(\lambda_{\odot,t_n} - \lambda)]\}}. \tag{5}$$

Using Eq. (5), we can evaluate the influence of this time correction on $f_{\mathrm{ny},n}$ (i.e., f_{ny}, hereafter denoted as $f_{\mathrm{ny},n}$ in a simplified way) for *Kepler* spacecraft. For simplicity, we solve Eq. (5) numerically by taking parameters of the *Kepler* spacecraft's orbit as their similarity. Table 1 lists the details of those parameters. We note that several parameters in this numerical solution are derived from *Kepler* observations. For instance, t_0 corresponds

Table 1. Input parameters for the numerical solution to f_{ny}.

Parameter	Value
t_0 (BKJD)	120
Δt (s)	1800
a (m)	1.516×10^{11}
e	0.036
$M_\odot$ (kg)	1.989×10^{30}
RA	$19^{\mathrm{h}}22^{\mathrm{m}}40^{\mathrm{s}}$
Dec	$+44°30'00''$

Notes. Start time, t_0, for the first data point, sampling interval Δt, semi-major axis a and eccentricity e of spacecraft's elliptical orbit, masses of the Sun $M_\odot$, and the right ascension (RA) and declination (Dec) of the pointing center in the *Kepler* field of view.

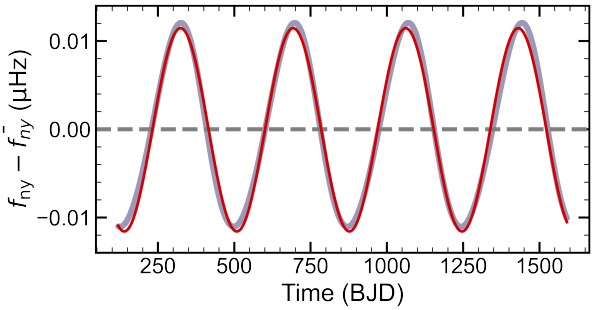

Fig. 1. Modulating pattern of f_{ny} derived from numerical calculation using *Kepler* long-cadence photometry. The gray dots (too dense) represent the numerical results, while the red solid curve denotes the fitting results. The dashed horizontal line indicates the mean value of f_{ny}.

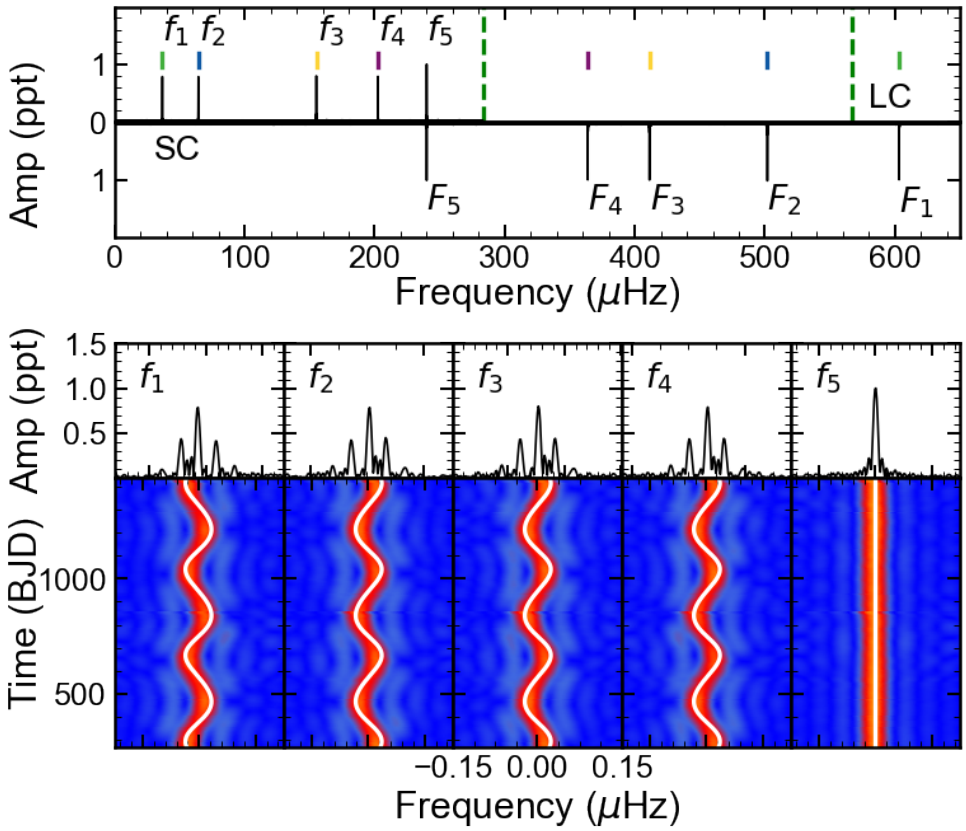

Fig. 2. LSP of the simulated photometry. Top panel: General view of the LSP, showing the frequencies injected into the simulated long- (upper) and short-cadence (lower) photometry, respectively. Middle panel: LSPs for the five detected frequencies. Bottom panel: Sliding LSP of the five detected frequencies corresponding to these five frequencies, as depicted in the middle panel.

to the same to the first data point of the long-cadence photometry for most γ Dor variables. Figure 1 illustrates the periodic modulation of $f_{\rm ny}$ around its mean value, with a peak-to-peak amplitude of approximately 0.02 μHz. A pure sinusoidal wave fits the variation pattern closely, indicating that the elliptic solution approximates a circular orbit. The nonlinear-least-squares fitting yields the following parameters: amplitude of 11.560 ± 0.005 nHz, period of ~373.547 ± 0.063 days and phase of 0.3972 ± 0.0001.

2.2. Simulation of super-Nyquist frequency variation

If a real frequency is higher than $f_{\rm ny}$, it is referred to as the super-Nyquist frequency, $f_{\rm sny}$. Here, we first examine the case, where $f_{\rm sny}$ falls within the frequency range $[f_{\rm ny}, 2f_{\rm ny}]$. In this scenario, $f_{\rm sny}$ will be reflected into the frequency range $[0, f_{\rm ny}]$ and the reflected frequency $f_{\rm ref}$ is

$$f_{\rm ref} = 2f_{\rm ny} - f_{\rm sny}. \quad (6)$$

Since we typically perform a Fourier transform of *Kepler* photometry up to the Nyquist frequency, it is easily to foresee that the detected frequency, $f_{\rm ref}$, as a reflection of $f_{\rm sny}$, should vary over time according to Eq. (6). Over the four-year *Kepler* observations, $f_{\rm sny}$ is expected to complete four cycles of frequency modulation; this process is now referred to as $f_{\rm sny}$ modulation or SNF modulation. In this work, we adopt SNF modulation as an independent technique to distinguish whether a frequency is reflected and originates from a higher $f_{\rm sny}$. We note that the modulating pattern of SNFs differs completely from the intrinsic modulation of pulsation modes. As documented in Zong et al. (2018), intrinsic modulation exhibits distinctive patterns, whereas SNF modulation is expected to be highly similar and strictly periodic. In cases where intrinsic modulation coincidentally exhibits a pattern similar to SNF modulation, the two may become indistinguishable.

We then conducted simulations to assess whether SNF modulation can be effectively characterized in practical *Kepler* long-cadence photometry. Short-cadence photometry is also been considered to compare the behavior of high frequency beyond $f_{\rm ny}$ of long-cadence data. Following a strategy similar to that of Zong et al. (2018, 2021), we produce artificial photometry involving time sampling, frequency injection and extraction, and the sliding Lomb-Scargle periodogram (sliding LSP). The time samplings are consistent with real pulsating stars, the γ Dor star KIC 2168333 and the white dwarf KIC 8626021 representing long- and short-cadence photometry, respectively. Table B.1 lists the five independent frequencies, $F_1 - F_5$, that were injected into the artificial light curves. As predicted, four frequencies are reflected below $f_{\rm ny} \sim 284$ μHz, except for F_5, which is below $f_{\rm ny}$ in long-cadence photometry. These five extracted frequencies are labeled as $f_1, f_2, \ldots f_5$ in the LSP of long-cadence photometry. Notably, f_1 is reflected twice, as the real injected frequency F_1 exceeds $2f_{\rm ny}$, as illustrated in Fig. 2. Except f_5, which exhibits a spike profile, all reflected frequencies display a multiplet structure in the LSP, consistent with the simulation of Murphy et al. (2013). The bottom panels of Fig. 2 show the sliding LSP for the five extracted frequencies from long-cadence photometry, using a window step of 5 days and a window length of 300 days. The first four frequencies clearly exhibit periodic modulations in frequency, completing three cycles over ~1000 days, while f_5 is stable throughout. The modulating patterns of f_2, f_3, and f_4 is identical and exhibit an anti-phase relationship with f_1. This occurs because $f_1 = F_1 - 2f_{\rm ny}$ is reflected twice, while the other three frequencies are reflected once; for instance, $f_2 = 2f_{\rm ny} - F_2$. Our simulations demonstrate that modulations of SNFs can be

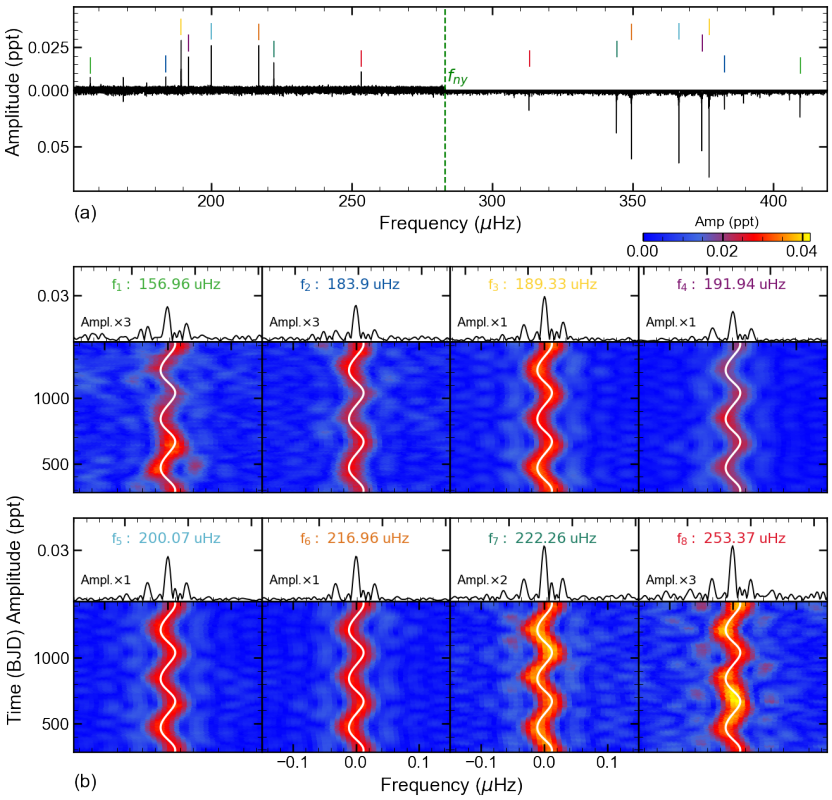

Fig. 3. LSP of the majority of detected frequencies and the sliding LSP of eight identified SNFs in KIC 9533489. (a) LSP of the majority of detected frequencies observed in both short- and long-cadence photometry. The vertical segments indicate the positions of the eight SNFs detected in long-cadence photometry, which have been confirmed through SC photometry. (b) Detailed view of the eight SNFs, where each panel displays both the LSP profile and the corresponding sliding LSP. Note: LSPs multiply a factor to improve their visibility by their relative amplitude. The solid curves represent the numerical predictions of SNF modulation, shown in comparison with the observational data.

effectively characterized based on the sliding LSP; namely, a behavior that is induced through time correction applied in *Kepler* photometry.

To evaluate the differences caused by beating effects, a factor that introduces amplitude modulation was included in a comparative simulation applied to *Kepler* photometry (see Appendix A.1). For comparison, we also performed a series of simulations with the same method, but extended to TESS photometry, given in Appendix A.2. These simulations suggest that our method of sliding LSP is better suited for nearly continuous photometry.

3. Photometric data and processing method

We directly adopted the catalog of 611 γ Dor stars constructed by Li et al. (2020) using *Kepler* photometry and collected the corresponding light curves with PDCSAP flux from the Mikulski Archive for Space Telescopes (Jenkins et al. 2010). Most of the targets were observed in long cadence of 30 minutes. Following the procedures outlined in Xing et al. (2024), the collected light curves were processed with quality checking, flux normalization, outlier clipping, and quarter combing, using the `lightkurve` package (Lightkurve Collaboration 2018); whereas the detrending procedure has done with `wotan` (Hippke et al. 2019). The cleaned light curves were then analyzed using the dedicated software `FELIX` to extract significant frequencies (for details, see Charpinet et al. 2010; Zong et al. 2016). For the frequencies of interest, we adopted a threshold of eight times the local noise level, allowing us to detect variations in SNFs using sliding the LSP. The previous section presents a series of simulations validating our method for efficiently identifying SNFs. As demonstrated in Sect. 2.2, we also analyzed the available one-minute short-cadence photometry to further validate the existence of SNFs.

Figure 3 provides an example illustrating the identification of SNFs in γ Dor star KIC 9533489. Figure 3a shows the Lomb-Scargle periodogram (LSP) for both long- and short-cadence light curves. Since this star has only two quarters of continuous short-cadence photometry, the number of significant frequencies detected is lower (36) compared to those found in 17 quarters of long-cadence photometry (56) over 8σ. However, the higher Nyquist frequency limit provided by short-cadence photometry can help verify the reality of SNFs detected in the LSP of long-cadence photometry. We detected eight SNFs using the sliding LSP with a 300-day window length and 5-day step, revealing periodic frequency variations, as shown in Fig. 3b. Each of these SNFs exhibits an LSP profile characterized by a modulating multiplet structure, as documented by Murphy et al. (2013). Evidently, all eight frequencies exhibit the same patterns and complete three full cycles during the *Kepler* observations. The modulating patterns also agree very well with those predicted by our numeric calculations (see Sect. 2.1 for details).

We applied the same method to identify SNFs in 12 γ Dor stars using both long- and short-cadence photometry, with detailed information presented in Table B.1. The results, along with simulations in Sect. 2.2, confirm the method's validity and feasibility for identifying SNFs through the sliding LSP based on periodic frequency modulation. We then applied this technique to the remaining ~600 stars, concentrating exclusively on the sliding LSP of their long-cadence photometry. However, the method is constrained to detecting frequencies with sufficient amplitude for reliable identification. Thus, our method provides only a lower bound on the number of detectable SNFs in γ Dor stars.

4. Results

We extracted 45607 frequencies with amplitudes high enough for sliding LSP analysis from the 611 γ Dor stars. Each star

Table 2. All 304 identified SNFs in 56 γ Dor stars.

KIC	$f_{\rm detect}$ (μHz)	σf (μHz)	Amp. (ppm)	σA (ppm)	$f_{\rm real}$ (μHz)
...	...	...	...	...	...
3456780	268.48212	0.00012	55.2	1.5	297.93988
3456780	279.75829	0.00018	35.6	1.5	286.66371
3456780	280.91340	0.00021	31.6	1.5	285.50860
3655115	267.81653	0.00004	460.5	4.4	298.60547
3655115	270.49416	0.00004	443.1	4.0	295.92784
3867256	213.58265	0.00025	60.1	3.5	352.83935
3867256	236.27909	0.00015	119.3	4.0	330.14291
3867256	258.88693	0.00025	73.1	4.2	307.53507
3867256	259.50234	0.00014	129.9	4.3	306.91966
3867256	264.88586	0.00005	393.1	4.4	301.53614
...	...	...	...	...	...

Notes. The frequency list is sorted by the KIC ID (Column 1) and frequency (Column 2). Column (3): Errors associated with the frequencies. Columns (4) and (5): Amplitudes and their associated errors. Column (6): Real frequencies corresponding to the SNFs. The full list can be accessed through an online version.

exhibits several dozens to hundreds of frequencies, which are available for further analysis. Using this method, we identified 304 SNFs in 56 stars after thoroughly examining the sliding LSP for all relevant frequencies. Table 2 lists details of these SNF frequencies. The number of SNFs per star varies from 1 to 10, typically with number of 5. Of the 304 SNFs, only two are located within the frequency range of g-mode pulsations in the γ Dor star KIC 8973529 and KIC 9766218.

Figure 4 illustrates both the LSP and sliding LSP for this specific frequency. Two primary groups of low-frequency g-modes have been observed in KIC 8973529. A close-up of the frequency around 38.94 μHz reveals a multiplet profile in the LSP. The sliding LSP around 38.94 μHz exhibits clear periodic frequency variation, with the pattern closely aligning with theoretical predictions (see details of numeric exploration in Sect. 2.1). However, a minor discrepancy between the initial theoretical calculations and the observational results is noted. This suggests the presence of intrinsic modulation in the pulsation mode, in addition to SNF modulation. A similar modulation is observed in KIC 9766218, where the frequency around 24.06 μHz also exhibits periodic variation. Notably, this modulation pattern differs in phase from the theoretical prediction. We tentatively identified this frequency as a SNF, although further investigation is required.

Apart from the two aforementioned frequencies, the remaining SNFs fall within the range of p-mode pulsations in hybrid γ Dor stars. The statistical distribution of relevant frequencies and SNFs is shown in Fig. 5. Consistent with theoretical predictions for γ Dor stars, the distribution of g-modes is dense, with most frequencies concentrated around 20−30 μHz. The number of frequencies gradually decreases as the frequency increases. The long tail of the distribution indicates that p-modes in hybrid γ Dor stars span a significantly broader frequency range. A notable feature is that the number of identified SNFs increases with frequency, representing a fraction rising from ∼1% to 7% up to the Nyquist frequency of long-cadence photometry. This indicates that SNFs are primarily reflection of high p-mode frequencies and only a few modes are excitable with frequencies exceeding the Nyquist frequency of *Kepler* long-cadence photometry in hybrid γ Dor-δ Scuti stars.

Figure 6 presents the distribution of these 611 stars on the Hertzsprung-Russell (HR) diagram. The effective temperature ($T_{\rm eff}$) and luminosity values for γ Dor stars are sourced from the catalog in Li et al. (2020). As depicted in the figure, the theoretical instability strips for γ Dor are adopted from Dupret et al. (2005), whereas the observational instability strips for δ Scuti stars are introduced by Murphy et al. (2019). The majority of stars with detected SNFs are situated outside the instability strip (IS) of γ Dor stars but within the IS of δ Scuti stars. This finding further supports the notion that SNFs correspond to p-modes in hybrid γ Dor-δ Scuti stars.

5. Discussion and summary

A primary objective of this study is to determine whether the reflection of SNFs affects the seismic patterns of g-mode in γ Dor variables. In this study, we identified only two candidate SNFs in the low g-mode region, with a false alarm probability of $p < 0.005\%$. This low probability suggests that SNFs have minimal impact on seismic patterns, such as the period spacing slope, as derived in previous studies (Van Reeth et al. 2016; Li et al. 2020; Ouazzani et al. 2020). Thus, the seismic properties derived from g-mode characteristics appear unaffected, despite the reflection of high frequencies into the lower-frequency region in *Kepler* long-cadence photometry. This result also indicates that p-mode frequencies in hybrid γ Dor stars rarely exceed 500 μHz. According to Eq. (6), only frequencies exceeding this value can appear in the g-mode region of γ Dor stars.

Although the two SNFs are generally aligned with the predicted patterns, a slight discrepancy is observed, particularly the frequency around 24 μHz in KIC 9766218. This frequency exhibits a phase difference between theoretical calculations and observational data (as shown in Fig. 4), calling for further interpretation. Unfortunately, neither of these two stars have been observed with short-cadence photometry, which would provide an independent verification of the presence of SNFs.

Many γ Dor stars exhibit both g- and p-mode pulsations, enabling both their inner core and outer envelope to be probed. Thus, pressure modes are also crucial to seismic modeling for γ Dor stars. Our results clearly indicate that most SNFs are likely reflections of p-modes. We find that the fraction of SNFs increases with frequency (Fig. 5), which can be attributed to the decreasing number of p-modes at higher frequencies, where the remaining modes are reflected by the Nyquist mirror effect. Our results suggest that the high-frequency p-modes over Nyquist frequency may remain undetected, resulting in some wrong mode discriminant in hybrid δ Scuti-γ Dor stars. Therefore, in hybrid γ Dor stars, it is essential to carefully inspect p-mode frequencies when incorporating them into seismic models. According to the distribution of SNFs, most p-mode SNFs are concentrated in the frequency range of 280−360 μHz, with few exceeding 400 μHz. They correspond to the low radial order p-modes in the δ Scut stars.

At this stage, it is important to note that frequencies in δ Scuti stars must be carefully examined, since they exhibit similarities to those found in hybrid γ Dor stars. Frequencies exceeding the Nyquist frequency of long-cadence *Kepler* photometry will be reflected and mixed with real p-mode frequencies, making mode discrimination more difficult. By analyzing the temporal behavior of pulsation frequencies, we can distinguish between SNFs and intrinsic modulations (Niu & Xue 2024). Our method is also applicable for identifying SNFs in other rapid pulsators, such as

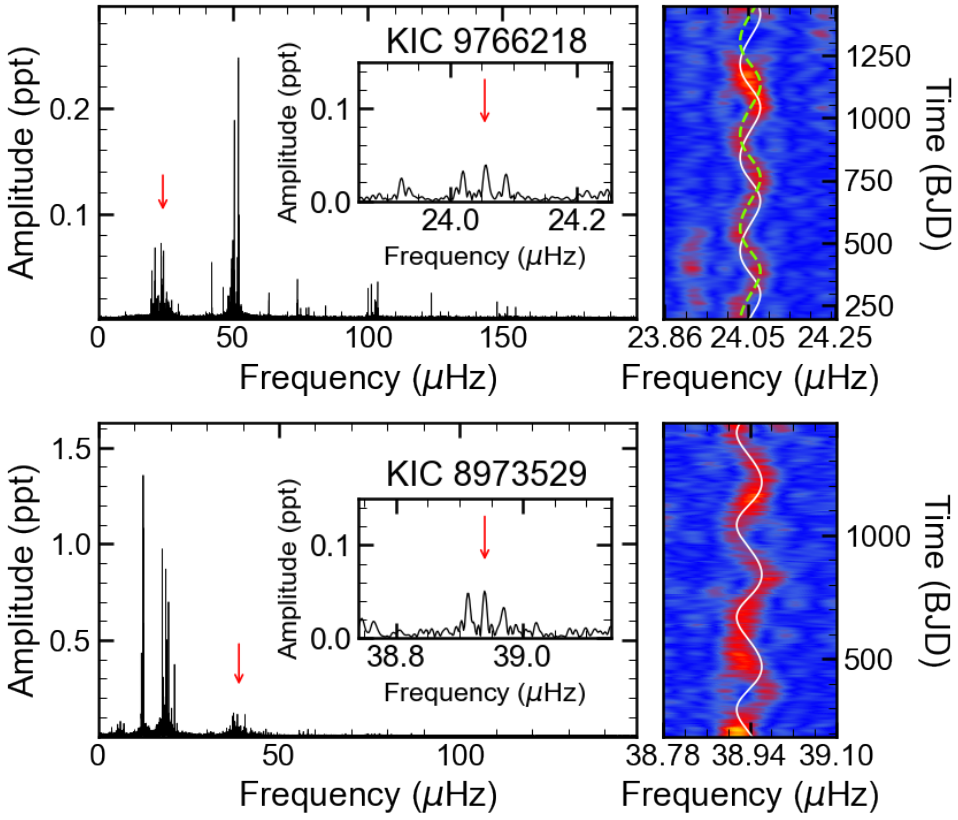

Fig. 4. Two high potential cases of SNFs in low frequency range for γ Dor stars. Left panels: LSP in the range where the majority of frequencies are detected. A close-up view of the SNF is zoomed inside. The red vertical arrow locates the SNF. Right panels: Sliding LSP, centered on the SNF, displays a periodic pattern of frequency modulation, which is compared with the theoretical variation of the SNF (solid curve) and a phase (π/2) shifted result (dashed curve).

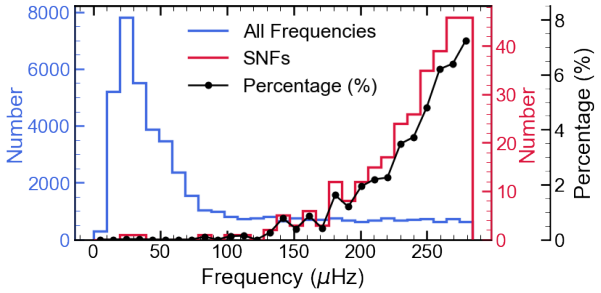

Fig. 5. Distribution of 45 607 frequencies detected in 611 γ Dor stars. The three vertical axes correspond to color-coded data. The blue line represents the distribution of all detected frequencies in the 611 γ Dor stars, while the red lines show the distribution of 304 SNFs. The black dots indicate the percentage of SNFs relative to all detected frequencies.

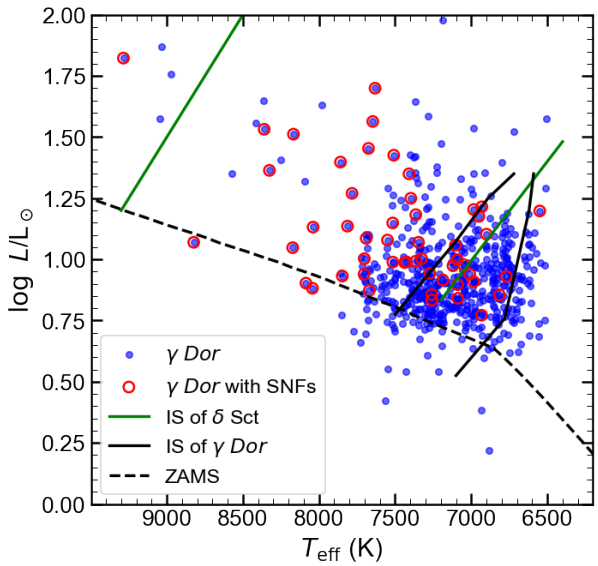

Fig. 6. HR diagram shows the distribution of 611 γ Dor variables. Blue dots represent all 611 γ Dor stars, while open red circles denote the 56 γ Dor stars with detected SNFs. The solid curves are instability strips of γ Dor stars and δ Scuti stars (see text for details). The dashed line indicates the Zero-Age Main Sequence (ZAMS).

sdB or roAp stars. However, in this study, we performed simulations only for *Kepler* long-cadence photometry. The pulsation in these rapid pulsators can even exceed the Nyquist frequency of short-cadence photometry. Similar to simulations presented here (see Sect. 2), further studies can be conducted for *Kepler* short-cadence photometry in the future.

As documented by Murphy et al. (2013), SNFs can be identified based on their characteristic equal-spacing multi-peaks in the LSP. However, this method may lead to false classifications if a star exhibits rotational multiplets with very similar frequency spacing. Both types of multiplet structure can coexist in a pulsating star. Our results demonstrate that the sliding LSP provides an independent method for confirming or refuting the presence of SNFs by analyzing their temporal frequency variations. Compared to a direct extraction of frequency modulation (Zong & Charpinet 2021; Bowman et al. 2016), the sliding LSP proves feasible for identifying SNFs and can be applied to a large sample of pulsating stars, including γ Dor. It does not require extensive computational resources to prewhiten all relevant frequencies. Concretely, with eight-core Apple M1@3.2GHz processor, our method takes approximately 20 s to construct the entire sliding LSP from the light curve in Sect. 2.2; whereas the prewhitening method takes over 220 s to process all five frequencies by `FELIX`. We note that the prewhitening method requires

significantly more computational time as the number of frequencies increases, unlike our method. The numerical pattern identified here can be directly utilized to verify SNFs based on their sliding LSP signatures. In practice, we recommend employing a combined approach of all three techniques for SNF identification in specific targets of interest, significantly enhancing the accuracy of detecting true SNFs.

We emphasize that SNFs must be examined a priori before conducting seismic analysis of pulsating stars using *Kepler* long-cadence photometry. In the future, we will apply SNF modulation to various types of pulsating stars and establish catalogs of known SNFs. This will facilitate and streamline future seismic analyzes. Additionally, our method can be extended to K2 and TESS photometry, as well as to upcoming missions such as PLATO (Rauer et al. 2014). Future works will also apply SNF modulation to *Kepler* and TESS short-cadence photometry to search for rapid pulsation frequencies. In conclusion, SNF modulation now serves as an independent technique that has the potential to advance asteroseismological studies for various types of pulsators in the future.

Data availability

A full version of Table 2 is available at the CDS via anonymous ftp to cdsarc.cds.unistra.fr (130.79.128.5) or via https://cdsarc.cds.unistra.fr/viz-bin/cat/J/A+A/693/A63

Acknowledgements. The authors acknowledge the support from the National Natural Science Foundation of China (NSFC) through grant Nos. 12273002, 12090040 and 12090042. This work is supported by the International Centre of Supernovae at Yunnan Key Laboratory (Nos. 202302AN360001 and 202302AN36000102) and the science research grants from the China Manned Space Project. S.C. has financial support from the Centre National d'Etudes Spatiales (CNES, France). T.W. acknowledges the support from the National Key Research and Development Program of China (grant No. 2021YFA1600402), the B-type Strategic Priority Program of the Chinese Academy of Sciences (grant No. XDB41000000), and the Yunnan Ten Thousand Talents Plan Young & Elite Talents Project. All of the *Kepler* and TESS data used in this paper can be found in MAST. The authors appreciate all who have contributed to making these missions possible. Funding for the *Kepler* and TESS mission is provided by NASA's Science Mission Directorate.

References

Aerts, C. 2021, Rev. Mod. Phys., 93, 015001
Baran, A. S., Reed, M. D., Stello, D., et al. 2012, MNRAS, 424, 2686
Bedding, T. R., Mosser, B., Huber, D., et al. 2011, Nature, 471, 608
Bell, K. J., Hermes, J. J., Vanderbosch, Z., et al. 2017, ApJ, 851, 24
Borucki, W. J., Koch, D., Basri, G., et al. 2010, Science, 327, 977
Bowman, D. M. 2020, Front. Astron. Space Sci., 7, 70
Bowman, D. M., Kurtz, D. W., Breger, M., Murphy, S. J., & Holdsworth, D. L. 2016, MNRAS, 460, 1970
Chaplin, W. J., Elsworth, Y., Davies, G. R., et al. 2014, MNRAS, 445, 946
Charpinet, S., Green, E. M., Baglin, A., et al. 2010, A&A, 516, L6
Dupret, M. A., Grigahcène, A., Garrido, R., Gabriel, M., & Scuflaire, R. 2005, A&A, 435, 927
Fuller, J., Cantiello, M., Stello, D., Garcia, R. A., & Bildsten, L. 2015, Science, 350, 423
Giammichele, N., Charpinet, S., Fontaine, G., et al. 2018, Nature, 554, 73
Guzik, J. A., Kaye, A. B., Bradley, P. A., Cox, A. N., & Neuforge, C. 2000, ApJ, 542, L57
Hey, D. R., Holdsworth, D. L., Bedding, T. R., et al. 2019, MNRAS, 488, 18
Hippke, M., David, T. J., Mulders, G. D., & Heller, R. 2019, AJ, 158, 143
Howell, S. B., Sobeck, C., Haas, M., et al. 2014, PASP, 126, 398
Huber, D., Chaplin, W. J., Christensen-Dalsgaard, J., et al. 2013, ApJ, 767, 127
Jenkins, J. M., Caldwell, D. A., Chandrasekaran, H., et al. 2010, ApJ, 713, L87
Kurtz, D. W. 2022, ARA&A, 60, 31
Li, G., Van Reeth, T., Bedding, T. R., et al. 2020, MNRAS, 491, 3586
Li, G., Deheuvels, S., Ballot, J., & Lignières, F. 2022, Nature, 610, 43
Lightkurve Collaboration (Cardoso, J. V. D. M., et al.) 2018, Astrophysics Source Code Library [record ascl:1812.013]
Ma, X.-Y., Zong, W., Fu, J.-N., et al. 2022, ApJ, 933, 211
Miglio, A., Chiappini, C., Mackereth, J. T., et al. 2021, A&A, 645, A85
Mosser, B., Dréau, G., Pinçon, C., et al. 2024, A&A, 681, L20
Murphy, S. J. 2015, MNRAS, 453, 2569
Murphy, S. J., Shibahashi, H., & Kurtz, D. W. 2013, MNRAS, 430, 2986
Murphy, S. J., Hey, D., Van Reeth, T., & Bedding, T. R. 2019, MNRAS, 485, 2380
Niu, J.-S., & Xue, H.-F. 2024, A&A, 682, L8
Ouazzani, R. M., Lignières, F., Dupret, M. A., et al. 2020, A&A, 640, A49
Rauer, H., Catala, C., Aerts, C., et al. 2014, Exp. Astron., 38, 249
Ricker, G. R., Winn, J. N., Vanderspek, R., et al. 2015, J. Astron. Telesc. Instrum. Syst., 1, 014003
Uytterhoeven, K., Moya, A., Grigahcène, A., et al. 2011, A&A, 534, A125
Van Reeth, T., Tkachenko, A., Aerts, C., et al. 2015, A&A, 574, A17
Van Reeth, T., Tkachenko, A., & Aerts, C. 2016, A&A, 593, A120
Xing, K., Zong, W., Silvotti, R., et al. 2024, ApJS, 271, 57
Zong, W., & Charpinet, S. 2021, Res. Notes Am. Astron. Soc., 5, 41
Zong, W., Charpinet, S., Vauclair, G., Giammichele, N., & Van Grootel, V. 2016, A&A, 585, A22
Zong, W., Charpinet, S., Fu, J.-N., et al. 2018, ApJ, 853, 98
Zong, W., Charpinet, S., & Vauclair, G. 2021, ApJ, 921, 37

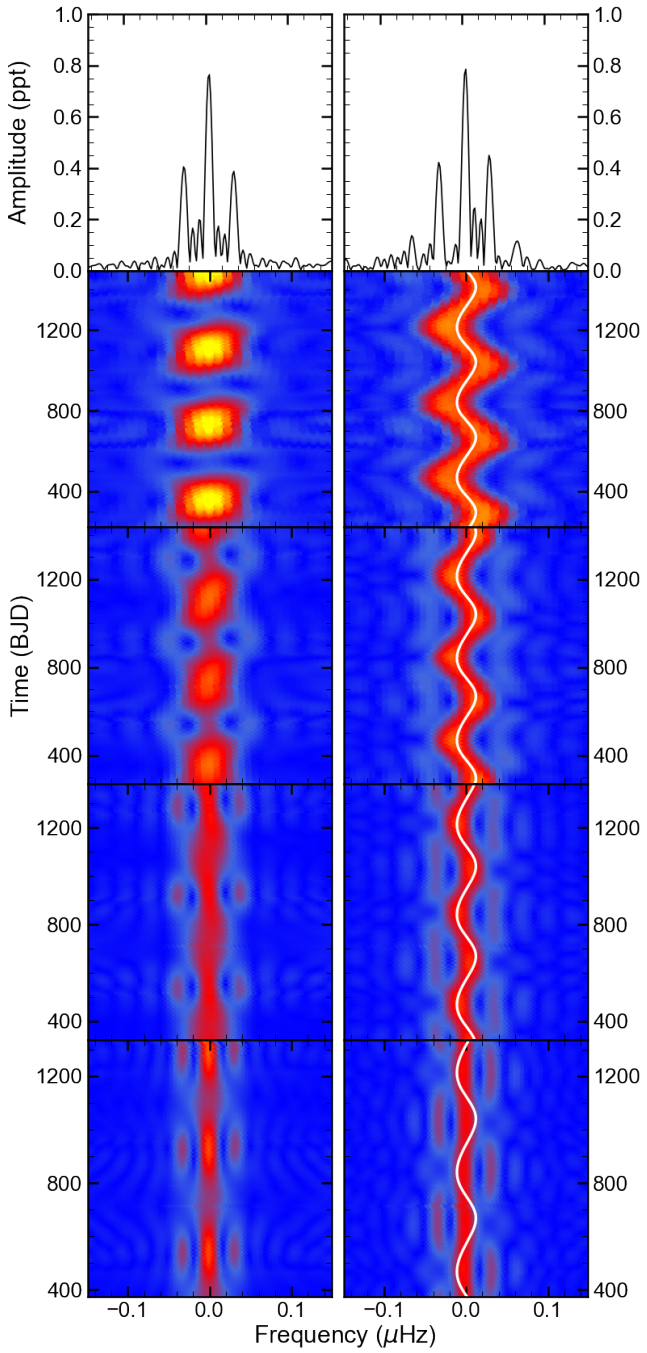

Fig. A.1. Comparison of modulating patterns between a close triplet (left panels) and a SNF (right panels). Topmost panels: LSPs for the two types of frequencies. Subsequent panels: Sliding LSPs with window lengths of 200, 300, 400, and 500 days, displayed from top to bottom. The window step is consistently set to one day across all simulations.

Appendix A: Additional simulation

A.1. Beating modulation versus SNF modulation

This section directly compares the modulation features of SNFs with those of closely spaced frequencies, such as an intrinsic triplet. Distinguishing a closely spaced multiplet from a modulated, split SNF using only the LSP is challenging. A pair of closely spaced frequencies will exhibit amplitude modulations in the sliding LSP if their frequency separation is smaller than the frequency resolution. This phenomenon is known as the beating effect. Following a similar methodology to Ma et al. (2022), we performed sliding LSP simulations on closely spaced frequencies with frequency separations equivalent to those of Nyquist splittings.

Figure A.1 presents a comparison between the modulation effects of beating and SNFs. It is evident that the triplet exhibits a distinctly different modulation pattern compared to the SNFs. The triplet shows stable frequency with noticeable amplitude modulation, while the SNFs display periodic frequency modulation with significantly shallower amplitude changes. As the window length increases from 200 to 500 days, the frequency modulation becomes less pronounced, with a reduction in the modulation scale. This can be attributed to the fact that a longer window provides a smoother frequency measurement, especially when the window length significantly exceeds the modulation period. These results suggest that SNF modulation can be effectively distinguished from closely spaced triplets using the sliding LSP method.

A.2. Simulation based on TESS data

Following a similar methodology, we performed simulations of SNF modulation applied to the TESS 2-minute photometry, using the time sampling of TIC 348841203. The primary difference between *Kepler* and TESS is the presence of large one-year gaps in TESS data as shown in Fig. A.2, which induces side lobes in the LSP profile. As with *Kepler*, the real frequency remains stable, while the three SNFs show clearly periodic variations, as revealed from their sliding LSPs, even across large observational gaps. However, the LSP profiles exhibit broader and more complex structures compared to the multiplet patterns observed in *Kepler*'s LSP, due to the length of exposure. These features aid in the identification of SNFs in rapidly pulsating stars, such as p-modes in sdB stars or g-modes in white dwarfs.

The above simulation is suitable for TESS targets with nearly continuous observations, or targets located within or near the continuous view zone of TESS, which accounts for only about 2% of TESS coverage. Therefore, to evaluate the limitations of our method, we extend the simulations with variants of photometric duration, suitable for TESS targets observed over a few sectors in one cycle. Figure A.3 shows the results of sliding LSPs for 2, 4 and 6 sectors. In each panel, the sliding window was set to half of the observational duration, and the step was set to 5 days. The frequency remains relatively stable for the simulation of 2 sectors, whereas frequency modulation on a small scale becomes visible for 4 sectors. Frequency modulation becomes more pronounced and easily identifiable for 6 sectors. This implies that a minimum of 4-sector photometry is necessary to meet the criteria via the sliding LSP method. This means that only targets within or near the continuous view zone of TESS can effectively utilize the sliding LSP method, covering about 4% of the entire TESS field. It is important to note that intrinsic modulation of pulsation modes may be mixed with the SNF modulation, as their timescales are comparable when only 4-6 sectors of photometry are used for the sliding LSP technique. In a safe way, SNFs can be identified from nearly continuous photometry through their temporal behaviors.

Appendix B: Supplementary material

Table B.1. Five injected frequencies extracted from simulations of long- and short-cadence photometry.

ID	Frequency (μHz)	σf (μHz)	Amplitude (ppt)	σA (ppt)	Cadence	$f-$Range ($f_{\rm ny}$)	Comments
f_1	36.785704	0.000065	0.791	0.012	LC	–	$F_1 - 2f_{\rm ny}$
f_2	64.504302	0.000064	0.792	0.012	LC	–	$2f_{\rm ny} - F_2$
f_3	155.154317	0.000065	0.800	0.012	LC	–	$2f_{\rm ny} - F_3$
f_4	202.534340	0.000067	0.787	0.012	LC	–	$2f_{\rm ny} - F_4$
f_5	240.000083	0.000045	1.000	0.010	LC	–	F_5
F_5	239.999933	0.000076	1.005	0.011	SC	[0, 1]	–
F_4	363.889997	0.000073	0.991	0.011	SC	[1, 2]	–
F_3	411.270008	0.000074	0.995	0.011	SC	[1, 2]	–
F_2	501.919993	0.000075	1.009	0.011	SC	[1, 2]	–
F_1	603.210073	0.000078	0.988	0.011	SC	[2, 3]	–

Notes. Columns are as follows: (1) the identification, (2) and (3) frequencies and errors, (4) and (5) amplitudes and errors, (6) cadence type (LC or SC), (7) frequency range, and (8) comments on the relationship between reflected frequency and real frequency.

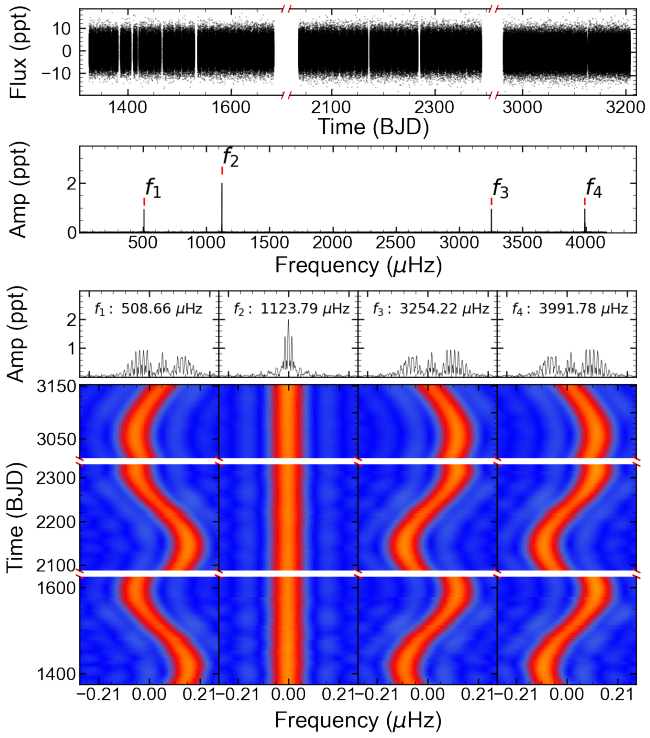

Fig. A.2. Simulation of SNF modulation using the time sampling of TIC 348841203 from TESS data. Top panel: Simulated light curve with a 120-second cadence, displaying amplitude in parts per thousand (ppt) of the mean brightness versus time. Middle panel: LSP displaying amplitude in ppt and frequency in μHz for the simulated light curve. Bottom panel: Sliding LSP of four significant frequencies identified in the LSP.

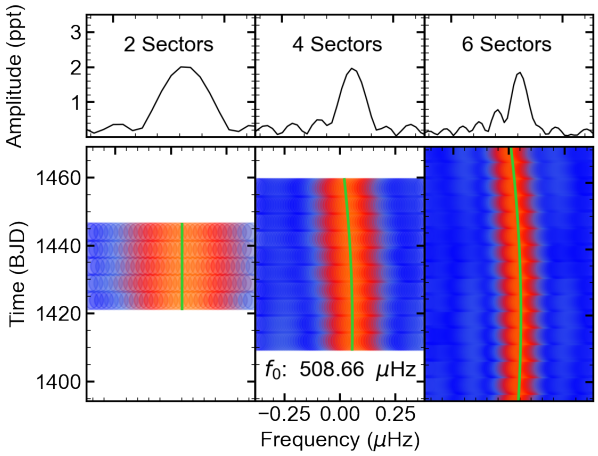

Fig. A.3. Modulation pattern of the SNFs across different numbers of sectors. From left to right: the data correspond to lengths of 2, 4, and 6 sectors. The green line represents a fitted line for frequency changes.

Table B.2. 12 γ Dor stars with identified SNFs also have been observed using *Kepler*'s short cadence.

KIC	$N_{\rm quarter}$	$N_{\rm SNF}$	$N_{\rm LC}$	$N_{\rm SC}$
2168333	1	8	509	47
3967333	1	6	238	52
4480321	1	3	212	10
5219533	1	1	333	10
5476864	1	1	73	10
6614168	1	1	283	26
7748238	6	2	203	102
7770282	1	2	16	45
7977996	1	19	583	59
9533489	2	8	56	36
9651065	2	17	430	273
10647493	1	1	47	116

Notes. $N_{\rm quarter}$ represents the number of quarters with short-cadence data; $N_{\rm snf}$ denotes the number of SNFs; N_{LC} denotes the number of frequencies detected in long-cadence data with a S/N greater than 8; and N_{SC} cdenotes the number of frequencies detected in short-cadence data with an S/N greater than 8.